

A Data Processing Approach to High Precision, High Return Rate kHz SLR Stations

John J. Degnan

Sigma Space Corporation, Lanham, MD USA

1. INTRODUCTION

The new kHz Single photon sensitive SLR stations are typically operated at low return rates (~10%) to minimize range biases due to “first photon effects”. Unfortunately, operation at low return rates partially negates one of the advantages of kHz systems, i.e. the ability to form accurate normal points more quickly, thereby reducing overall data volume by an order of magnitude or more and limiting the ability to move rapidly between satellites. At the 2017 ILRS Technical Workshop in Riga, the author proposed that the use of centroid detection circuits, instead of legacy threshold detection receivers, would allow the rapid production of bias-free normal points independent of signal return rates. The present paper investigates an alternative software approach for removing rate-dependent range bias which is applicable to commonly used threshold detection systems.

Signal detection is modelled as a Two State Markov Process, and the return rate within a given Normal Point (NP) is used, via Poisson statistics, to estimate the number of 1, 2, 3..etc photoelectron events contributing to the NP and to correct for the range bias. The single photon Probability Distribution Function (PDF) for the instrument ranging to a target (i.e. calibration or satellite) can be obtained theoretically or experimentally and used to correct for biases at high return rates.

2. PHOTOELECTRON DISTRIBUTION VS NP RETURN RATE

For an SLR receiver having a single photon detection threshold, the probability of detecting the satellite signal is given by Poisson statistics as

$$P_D = 1 - \exp(-\eta) \quad (1)$$

where η is the mean number of photoelectrons detected per pulse. Solving for η yields

$$\eta = \ln\left(\frac{1}{1-P_D}\right) \quad (2)$$

From Poisson statistics, the probability that a given return within the NP consists of n photoelectrons when the mean number is η is given by

$$P(n, \eta) = e^{-\eta} \frac{\eta^n}{n!} \quad (3)$$

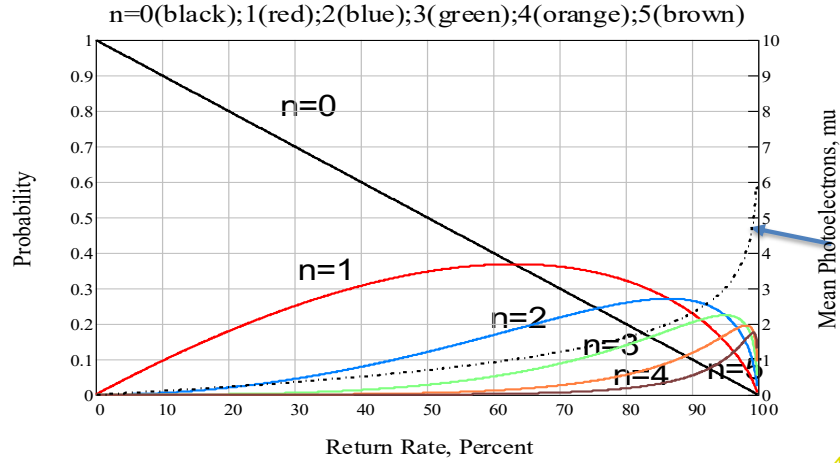
Using Eqs. (1) and (3) and the fact that the return rate is given by $RR = P_D(100\%)$ we can generate the graphs in Figure 1.

3. SGSLR LINK EQUATION

As demonstrated in this section, there are many operational scenarios where high return rates can be expected for the newsingle photon sensitive, kHz NASA Space Geodesy Satellite Laser Ranging (SGSLR). To compute the expected satellite return rates, we use a comprehensive link equation

$$n_s = \frac{E_t}{h\nu} \eta_t \frac{2}{\pi(\theta_d R)^2} \exp\left[-2\left(\frac{\Delta\theta_p}{\theta_d}\right)^2\right] \left[\frac{1}{1 + \left(\frac{\Delta\theta_j}{\theta_d}\right)^2} \right] \left(\frac{\sigma_{A_r}}{4\pi R^2}\right) \eta_r \eta_c T_a^2 T_c^2 \quad (4)$$

which includes relevant station and satellite parameters, telescope pointing bias and jitter, atmospheric visibility, mean cirrus cloud transmission, atmospheric turbulence effects and target speckle [Degnan, TBD] as listed in Table 1. The resulting plots of Probability of Detection, PD, for three representative satellites (Starlette, LAGEOS, and GNSS), as a function of satellite zenith angle and atmospheric visibility are presented in Figure 2. As one can see from Figure 2, there are numerous operating conditions, even for GNSS satellites at roughly 20,000 km altitudes, where the expected return rate far exceeds the “bias free” value of 10%.



4

Figure1: Left Axis-Probability of detecting n photoelectrons (n= 0 to 5) as a function of Return Rate within the Normal Point. Right Axis-Dashed curve indicates the mean photoelectrons detected vs Return Rate.

VARIABLE	SYMBOL	SGSLR VALUE
Laser Pulse Energy	E_t	1.5 mJ (60% of Max)
Laser Repetition Rate	f_L	2 kHz
Transmit Optics Efficiency	η_t	0.766
Receive Optics Efficiency	η_r	0.542
Detector Counting Efficiency	η_c	0.28
Spectral Filter Efficiency	η_f	0.7
Effective Receive Aperture	A_r	0.187 m ²
Tracking Pointing Bias	$\Delta\theta_p$	2 arcsec (Sigma Range Receiver)
Telescope RMS Pointing Jitter	$\Delta\theta_j$	2 arcsec
Full Transmitter Divergence	$2\theta_d$	28 arcsec (Starlette, LAGEOS) 14 arcsec (GNSS)
Coherence Length	ρ_0	20 cm (Excellent Site) 10 cm (Good Site) 2.5 cm (Poor Site)

Table 1. List of SGSLR and atmospheric parameters used in the link analysis.

4. PROBABILITY DISTRIBUTION FUNCTION (PDF)

The PDF for the photon time of arrival at the receiver is obtained by convolving the PDFs of the laser (L), the target (T), and the receiver (R), i.e

$$\lambda(t) = L * T * R \quad (5)$$

Thus, the photoelectrons arriving at the receiver have a PDF given by

$$\lambda(t) = \int_{-\infty}^t dt' R(t-t') \int_{-\infty}^{t'} dt'' L(t''-t) T(t'-t'') \quad (6)$$

which, for a single retro range calibration target reduces to

$$\lambda_c(t) = \int_{-\infty}^t dt'R(t-t') \int_{-\infty}^{t'} dt''L(t'')\delta(t'+\tau_c-t'') = \int_{-\infty}^t dt'R(t-t')L(t'+\tau_c) \quad (7)$$

where τ_c is the roundtrip flight time to the target. The instrument PDF due to the laser and receiver, $\lambda_c(t)$, can be measured at the output of the detector with a high speed oscilloscope or, for ultrashort pulses, a sampling scope, but we will also provide an experimental alternative for determining $\lambda_c(t)$.

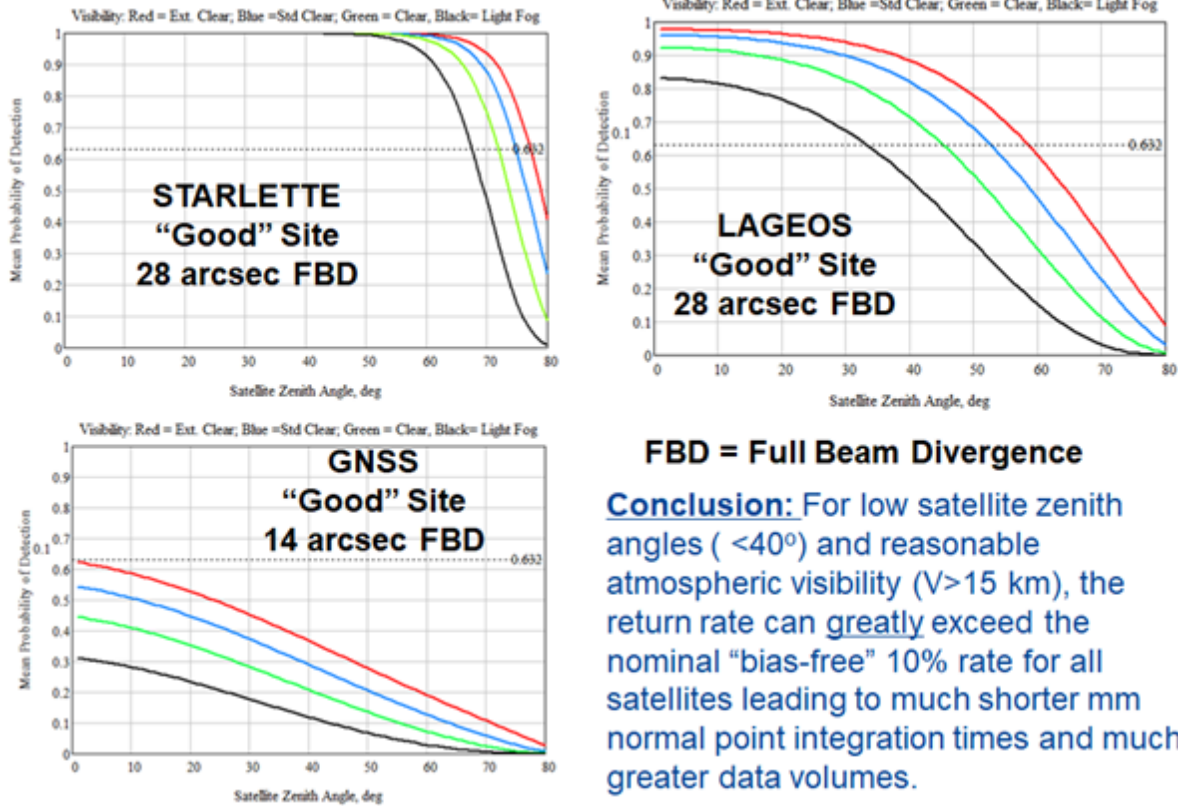


Figure 2: Mean Probability of SGSLR detecting three representative satellites (Starlette, LAGEOS, and GNSS) as a function of satellite zenith angle and four atmospheric visibilities: V=60 km Extremely Clear-red), 23 km (Standard Clear-blue), 15 km (Clear-green) and 8 km (Light Fog-black). A "Good Site" with an atmospheric coherence length $\rho_0 = 10$ cm was used to characterize the impact of atmospheric turbulence on beam propagation. For an "excellent" astronomical site, $\rho_0 = 20$ cm.

5. DETECTION AS A TWO STATE MARKOV PROCESS

Threshold detection can be treated as a Two State Markov Process (Degnan, 1994) with the initial state being "no detection" and the final state being "detection" (if $n>0$). The time of detection PDF depends on the detection threshold, T , the number of photoelectrons detected, n , and the n -photon temporal PDF distribution $\lambda(t)$ given by

$$P_n(t) = \frac{1}{1 - e^{-n}} a(n, T, t) \exp \left[- \int_{t_0}^{t_f} dt' a(n, T, t') \right] \quad (8)$$

where

$$a(n, T, t) = n\lambda(t) \frac{[n\lambda(t)]^{T-1}}{(T-1)!} \left\{ \sum_{k=0}^{T-1} \frac{[n\lambda(t)]^k}{k!} \right\}^{-1} \quad (9)$$

For a single photon detection threshold ($T = 1$) as in kHz SLR systems, $a(n, 1, t) = n\lambda(t)$ and

$$P_n(t) = \frac{\mu_n(t)}{1 - e^{-n}} = \frac{1}{1 - e^{-n}} n\lambda(t) \exp \left[-n \int_{t_0}^t \lambda(t') dt' \right] \quad (10)$$

where $\lambda(t)$ has a non-zero value only in the time interval $t_0 < t < t_f$ and the integral of $\lambda(t)$ over that interval is equal

to 1. Furthermore, once $\lambda(t)$ is known, the functional form of $\mu_n(t)$ is determined for all values of n .

For a normal point generated with multiple values of n and having a mean signal strength η , the bias in the photon time of detection is

$$\Delta t(\eta) = \langle t(\eta) \rangle - \langle t_0 \rangle = \sum_{n=1}^{\infty} P(n, \eta) \langle t_n \rangle - \langle t_0 \rangle = e^{-\eta} \sum_{n=1}^{\infty} \frac{\eta^n}{n!} \langle t_n \rangle - \langle t_0 \rangle \quad (11)$$

where the centroid of the PDF for n detected photoelectrons is given by

$$\langle t_n \rangle \equiv \int_{t_0}^{t_f} dt t P_n(t) = \frac{1}{1 - e^{-n}} \int_{t_0}^{t_f} dt t \mu_n(t) = \frac{n}{1 - e^{-n}} \int_{t_0}^{t_f} dt t \lambda(t) \exp \left[-n \int_{t_0}^t \lambda(t') dt' \right] \quad (12)$$

which, in the limit as n goes to zero, reduces to the unbiased photon arrival time

$$\langle t_0 \rangle = \int_{t_0}^{t_f} dt t \lambda(t) \quad (13)$$

6. DETERMINING $\lambda(t)$ EXPERIMENTALLY

One can measure the function $\lambda(t)$ from range data to the calibration target (or even a satellite by utilizing a low return rate (<10%) such that one is always seeing single photon returns. In this instance, the PDF of the measured ranges should obey the functional form

$$P_1(t) = \frac{\mu_1(t)}{1 - e^{-1}} = \frac{1}{1 - e^{-1}} \lambda(t) \exp \left[-\int_{t_0}^t \lambda(t') dt' \right] \quad (14)$$

where $t_0 < t < t_f$ and t_0 and t_f are defined as the end points of the $n=1$ detection PDF where $\lambda(t)=0$. Figure 3 shows the unsmoothed single photon PDF, $P_1(t)$, for NASA's prototype NGSLR station ranging to the calibration target.

The profile $P_1(t)$ can be smoothed (for example) by: (1) computing the Fourier Transform, (2) applying a bandpass filter to eliminate high frequency noise, and then (3) computing the inverse Fourier transform to provide the function $\mu_1(t)$ in tabulated or functional form. This can then be used to compute $\lambda(t)$ and the PDFs, $P_n(t)$, for a small range of n values and correct for biases in all future measurements to the same calibration target or satellite. We begin by computing $\mu_1(t)$ from the observed single photon PDF $P_1(t)$

$$\mu_1(t) = (1 - e^{-1}) P_1(t) \equiv \lambda(t) \exp \left[-\int_{t_0}^t \lambda(t') dt' \right] = -\frac{d}{dt} \exp \left[-\int_{t_0}^t \lambda(t') dt' \right] \quad (15)$$

Integrating both sides of the equation with respect to t yields

$$\exp \left[-\int_{t_0}^t \lambda(t') dt' \right] = 1 - \int_{t_0}^t \mu_1(t') dt' \quad (16)$$

and computing the logarithm of both sides gives

$$\int_{t_0}^t \lambda(t') dt' = \ln \left(\frac{1}{1 - \int_{t_0}^t \mu_1(t') dt'} \right) \quad (17)$$

and differentiating both sides with respect to t yields our final result

$$\lambda(t) = \frac{\mu_1(t)}{1 - \int_{t_0}^t \mu_1(t') dt'} \quad (18)$$

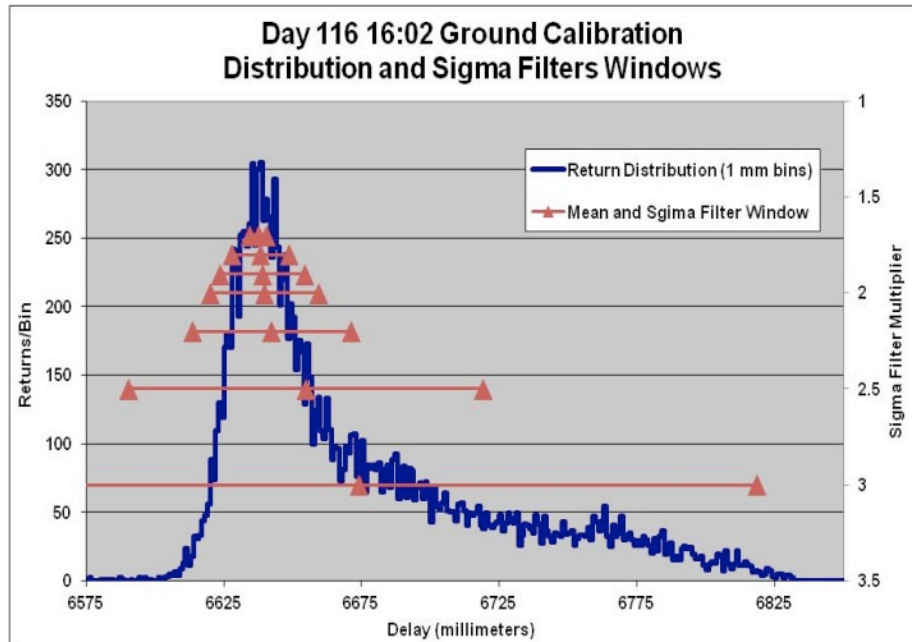


Figure 3: Unsmoothed Probability Distribution Function P1(t) of NASA's NGLSR system ranging to a single cube corner calibration target.

7. CORRECTING THE NORMAL POINT RANGE BIAS AT HIGH RETURN RATES

The blue curve in Figure 4(a) is the smoothed version of the Probability Distribution Function P1(t) in Figure 3 while the red curve is the photon arrival PDF, $\lambda(t)$, derived using Eqs. (14) and (18). The linear plot in Figure 4(b) is the expected range bias as a function of the return rate as computed from Eq.(11). Finally, in Figure 4(c), the measured range to the calibration target (brown curve – left axis) decreases as the return rate per one minute bin increases from a few percent to about 55% (blue curve-right axis). The red curve is generated by adding the negative range bias in 4(b) to the measured range at very low return rates which results in good agreement between the measured (brown) and corrected (red) ranges

8. SUMMARY

We have proposed both a theoretical and an experimental method for correcting the range bias in a normal point for an arbitrary return rate. This method not only provides a potentially bias-free range measurement but also removes the restriction to use only low return rates thereby greatly: (1) reducing the integration time for normal point generation and reducing the length of the orbital path which defines that normal point; (2) enhancing satellite data volumetric output in kHz SLR systems; and (3) Speeding up the interleaving of satellites.

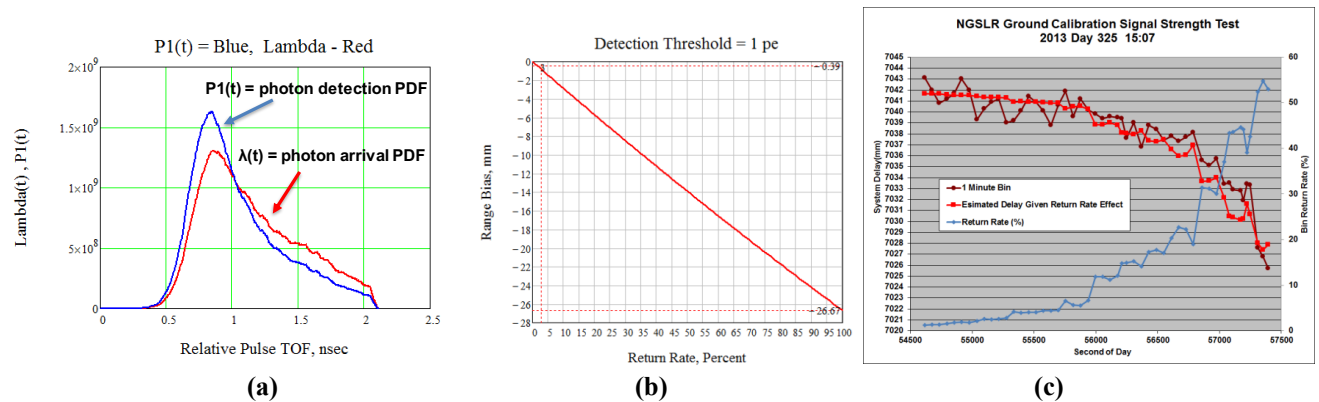


Figure 4: (a) Red $\lambda(t)$ curve derived from the blue experimental photon detection PDF, $P_1(t)$, to a single cube corner calibration target having a delta function optical response; (b) the derived theoretical range bias introduced by a growing return rate has a linear slope given by $\Delta R_C = -26.7 \text{ mm}(P_D)$ which can be explained by the substitution of $e^{-n} = (1-P_D)$ from Eq (1) into (11); (c) the agreement between the measured range (brown) with the corrected range (red) as the return rate in one minute samples is increased from a few percent to about 55% (blue). Similar analysis of NGSLR to LAGEOS data over a wide range of return rates also resulted in a linear range bias given by $\Delta R_L = -28.5 \text{ mm}(P_D)$ (see accompanying power point presentation).

The **theoretical method** determines the function $\lambda(t)$ by convolving the known PDFs for the laser, target, and receiver and then uses the result to compute the various PDFs associated with higher values of n and their corresponding time or range centroids, t_n . A theoretical model applicable to spherical satellites has been presented previously by the author (Degnan, 1993) and in the accompanying PowerPoint presentation for this Workshop. The **experimental method** uses low return rate measurements (<10%) to a particular target (calibration or satellite) to determine the single pe PDF $P_1(t)$ for that target and again uses that result to compute the PDFs and centroids for higher values of n . High frequency noise in the experimental data can be removed by a smoothing method, e.g. computing the Fourier transform, applying a bandwidth filter, and performing an inverse Fourier Transform. The approach assumes that the target response is largely independent of viewing angle, as with uniformly populated spherical geodetic satellites (LAGEOS, Starlette, etc.) or remote sensing or GNSS satellites where legacy flat panel arrays are replaced by segments of uniformly populated spheres (Degnan, 2016). Our results to date using NGSLR data suggest that the range bias is expected to vary linearly from 0 at very low return rates to a maximum on the order of -27 mm at very high return rates near 100%. Thus, two bias measurements at a very low and very high rate can define the bias at all rates.

ACKNOWLEDGEMENT. The author wishes to thank Christopher B. Clarke of KBRwyle for smoothing the low data rate NGSLR returns from the calibration target and from the LAGEOS satellite for the determination of $\mu_1(t)$ in both cases and plotting the final comparisons of the experimental high signal data biases with the theoretical predictions in Figure 4.

REFERENCES

Degnan, J, "Effects of Detection Threshold and Signal Strength on LAGEOS Range Bias", 9th International Workshop on Laser Ranging, Canberra Australia, 1994.

Degnan, J., "Millimeter Accuracy Satellite Laser Ranging: A Review", Contributions of Space Geodesy to Geodynamics: Technology, D. E. Smith and D. L. Turcotte (Eds.), AGU Geodynamics Series, Volume 25, pp. 133-162, 1993

Degnan, J. "Reducing the Satellite Contribution to Range Error", 20th International Workshop on Laser Ranging, Potsdam, Germany, October 2016.